Strong adsorption of phosphate by amorphous lanthanum carbonate nano-adsorbents

Yifan Lu, Huawei Wu, Yan Xia and Mei Huang

ABSTRACT

Phosphorus removal is a crucial aspect of controlling water pollution and eutrophication. In this study, the preparation of lanthanum carbonate (LC) nano-adsorbents for the efficient removal of phosphate (P) from water and wastewater was investigated. Results from XRD, SEM and Zeta potential analyses revealed that addition of magnesium ions and adjustment of the reaction temperature could control the morphology and microstructure of LC. Effects of initial pH, adsorbent dosage, contact time, and the water matrix on P adsorption were investigated. Batch adsorption experiments revealed that LC showed strong performance on P removal over a wide pH range (3.0 to 11.0). The kinetic data followed a pseudo-second-order model, and equilibrium data were well fitted by the Langmuir model with a maximum adsorption capacity of 112.9 mg P/g. Adsorption thermodynamics showed that the adsorption process was exothermic and spontaneous. Results of a monolayer model for single adsorption indicated that P could completely interact with two or more functional groups from the LC surface. In the presence of competing ions (F^-, Cl^-, SO_4^{2-}, NO_3^-, and HCO_3^-), LC maintained high selectivity for phosphate. For a real effluent, the P concentration was efficiently reduced from 3.2 mg P/L to below 0.5 mg P/L at a dose of 0.5 g/L LC. All the results suggested that LC can serve as a promising adsorbent for P removal in a wide range of pH, and thus could meet the stricter discharge regulations from actual wastewater.

Key words | adsorption kinetics, amorphous lanthanum carbonate, Langmuir model, nano-adsorbents, phosphate removal, water treatment

Yifan Lu
Huawei Wu
Yan Xia
Mei Huang (corresponding author)
College of Chemical & Biochemical Engineering,
Zhejiang University,
Zheda Road, Hangzhou 310027,
China
E-mail: *huangm@zju.edu.cn*

Mei Huang
Institute of Zhejiang University – Quzhou,
78 Jiuhua Boulevard North, Quzhou 324000,
China

HIGHLIGHTS

- High phosphate binding efficiency of amorphous lanthanum carbonate.
- The affinity of lanthanum carbonate nano-adsorbents toward phosphate was high over a pH range of 3.0–11.0.
- The Langmuir adsorption maximum for phosphate reached 112.9 mg P/g.

INTRODUCTION

Phosphorus (P) is a key nutrient that supports the growth of organisms in natural ecosystems. However, excessive release of P into water bodies can lead to eutrophication, which may cause excessive growth of algae, depletion of dissolved oxygen, deterioration of water quality, death of fish and plants, and other serious environmental problems (Correll 1998; King *et al.* 2015; Ding *et al.* 2018). Since the discharge of industrial wastewater and agricultural runoff are the primary causes of increased P concentrations in aquatic ecosystems, many countries and regions have enforced stricter P discharge limits to reduce the concentration of P in receiving water bodies and prevent eutrophication (Dodds *et al.* 2009; Karydis & Kitsiou 2012). For example, the United States

doi: 10.2166/wst.2021.086

Environmental Protection Agency (USEPA) recommends that any streams entering a lake or reservoir should have a total P concentration not exceeding 0.05 mg P/L, and the European Union (EU) defines the cut-off for total P concentration in lakes as non-risk and risk conditions of eutrophication to be <0.01 mg P/L and >0.1 mg P/L, respectively (Loganathan *et al.* 2014). For discharge from wastewater treatment plants, the permissible concentration of P will be lowered from 1–2 mg P/L to 0.1 mg P/L in the EU under the Water Framework Directive (Shepherd *et al.* 2016). Therefore, the selective and effective removal of P has become a challenge in the treatment of P-containing water and wastewater and has attracted considerable research interest in recent years.

Several technologies and processes, including biological, chemical, and physical treatments, have been developed for the removal of P from water and wastewater. Biological methods such as conventional activated sludge processes can achieve nearly 100% removal of P. However, these processes are less effective for P at trace levels, because such levels of P are below the metabolic thresholds of microorganisms (Sidat *et al.* 1999; Dulekgurgen *et al.* 2003). Moreover, higher capital cost and maintenance are often needed during implementation of biological methods, and sludge production then becomes a concern. Therefore, chemical treatments are primarily utilized in P removal, but these methods suffer from difficulties in sludge disposal and effluent neutralization. Physical methods such as reverse osmosis and electrodialysis, have been demonstrated to be either too expensive or inefficient in P removal (Wang *et al.* 2013; Seminskaya *et al.* 2017). The adsorption process is promising for P removal due to its attractive advantages, such as simple operation, high removal efficiency, and fast adsorption rate, especially at low P concentrations (Chouyyok *et al.* 2010; Yang *et al.* 2011). Many inorganic and organic adsorbents, as well as industrial by-products and biological wastes have been tested for their efficacy in removing P from wastewater. The main disadvantage of these adsorbents is their limited ability to adsorb P, even if the ratio of adsorbent to P varies between 100:1 and 1,000:1 (Yan *et al.* 2010; Yue *et al.* 2010; Hussain *et al.* 2011). Another disadvantage of using an adsorption method is that the adsorbed P may leach back into the solution after a period of time, causing concerns about secondary pollution (Bhardwaj *et al.* 2014).

Lanthanum-based adsorbents are rare-earth metal-based adsorbents with high chemical stability that are gaining increasing attention regarding the adsorption of P from water and wastewater due to their high affinity for P, even at low P concentrations. Moreover, the lanthanum–phosphate complex has been found to be stable in the pH range 3–6, with no detectable release of P or its solubility products (Aneesh *et al.* 2009). Therefore, various lanthanum materials have been prepared and investigated for P adsorption; for example, lanthanum hydroxide ($La(OH)_3$), La(III) oxide (La_2O_3) and a variety of lanthanum-incorporated materials (Li *et al.* 2009; Tian *et al.* 2009; Zhang *et al.* 2011; Liu *et al.* 2013; Spears *et al.* 2013; Xie *et al.* 2014a, 2014b; He *et al.* 2016; Wang *et al.* 2016). Although these adsorbents are highly efficient in reducing P concentrations to trace levels, there are still some limitations that inhibit their wide application. For example, these adsorbents exhibit high P adsorption capacity only under acidic conditions, so their performance will be greatly reduced when treating sewage under neutral and alkaline conditions. Therefore, in recent years, it has been desirable to obtain new lanthanum-based adsorbents with enhanced adsorption capabilities over a wider pH range to overcome these disadvantages.

Unlike the widely used lanthanum salts, such as $La_2(SO_4)_3$, $La(NO_3)_3$, $La(OH)_3$ and La_2O_3, LC has attracted intensive research interest in medical applications (Shao *et al.* 2011; Lee *et al.* 2013; Oka *et al.* 2016). LC is not only an effective P binder in the treatment of hyperphosphatemia of chronic kidney disease (CKD) (Behets *et al.* 2004; Tonelli *et al.* 2010) but is also tolerated by patients in long-term treatment (Guo *et al.* 2013; Hutchison *et al.* 2016). Being different from $La_2(SO_4)_3$ and $La(NO_3)_3$, the insolubility of LC results in low leaching of lanthanum ions during the adsorption process and thus is beneficial to the P removal in practical applications. Moreover, the pH buffering capacity of carbonate can limit the pH changes in the solution and keep the water body stable.

Based on previous studies of LC adsorbents for P removal from water and wastewater, the objectives of our work were to: (1) prepare an amorphous lanthanum carbonate adsorbent (simplified as LC) in co-existing Mg^{2+} through a facile coprecipitation method under different temperatures; (2) investigate the P adsorption performance (e.g., adsorption isotherms, adsorption kinetics, adsorption thermodynamics, physical models, effects of pH and co-existing ions); and (3) elucidate adsorption mechanisms of LC using a combination of XRD, FTIR and SAED analyses.

MATERIALS AND METHODS

Materials

All the chemicals used in this study were of analytical grade and were used without further purification. Lanthanum

chloride hexahydrate ($LaCl_3{\cdot}6H_2O$) was provided by Aladdin Chemical Reagent Co., Ltd (Shanghai, China). Anhydrous sodium bicarbonate ($NaHCO_3$) and magnesium sulphate heptahydrate ($MgSO_4{\cdot}7H_2O$), sodium hydroxide (NaOH) and anhydrous potassium dihydrogen phosphate (KH_2PO_4) were obtained from Shanghai Hushi Laboratory Equipment Co., Ltd (Shanghai, China). Deionized water was used throughout the study.

Synthesis of LC nano-adsorbents

LC nano-adsorbent was synthesized via a conventional coprecipitation method. The Mg^{2+} solution ($MgSO_4$) was added to a 0.04 M La^{3+} solution ($LaCl_3$) with a molar ratio (Mg^{2+}/La^{3+}) of 0.05:1, 1:1, 2.5:1 and 10:1 at different temperatures (298 K, 313 K, 328, 343 and 358 K). A slow drip of 0.12 M $NaHCO_3$ was added continuously for 30 min to the solution while stirring and to maintain the pH value of the solution at approximately 11. When the precipitation reaction was complete, the mixed products were centrifuged at a speed of 5,000 r/min for 10 min and subsequently washed thoroughly with deionized water until the pH of the effluent solution was neutral. Finally, the washed samples were oven-dried at 318 K for 12 h to obtain the corresponding LC adsorbents. Using the same process as above, a reference sample of lanthanum carbonate, simplified as LC_0, was obtained without the coexistence of Mg^{2+}.

Nano-adsorbents characterization

Scanning electron microscopy (SEM, HITACHI SU8010, Japan) was used to investigate the surface morphology of the different adsorbents synthesized. The crystal structures of the nano-adsorbents were analyzed using a Bruker D8 Advance diffractometer (X'Pert Powder, PANalytical, Netherlands) with Cu Ka radiation (40 kV, 40 mA) over the 2θ range of 10–60°. The zeta (ζ) potential of the prepared nano-adsorbents was measured using a Zetasizer 3000HSA (Malvern Instrument Ltd, UK). SAED patterns were obtained by using a transmission electron microscope (TEM, HITACHI HT-7700, Japan) operated at an acceleration voltage of 200 kV. The functional groups of adsorbents were recorded on an FTIR spectrometer (Nicolet 5700, USA) in the range of 4,000 cm^{-1} to 400 cm^{-1} using the KBr tablet method.

Adsorption evaluation

A series of batch experiments were carried out to investigate the adsorption behavior of P onto LC. About 0.02 g of LC was put into a flask containing 100 mL P solution ranging from 20 to 50 mg P/L. The suspensions in the covered flasks were shaken in a thermostatic chamber at a specified temperature for 24 h at 250 rpm. After 24 h, the equilibrium pH was measured, and the suspensions were centrifuged. The supernatant was collected through filtration using a 0.45 μm syringe filter and analyzed to determine the residual P concentration by the Mo-Sb anti-spectrophotometer method using a UV-vis spectrophotometer (HACH DR900, American).

The adsorption capacity (q_e, mg/g) and removal efficiency (E, %) of P were calculated from the respective equations:

$$q_e = \frac{(C_0 - C_e)V}{m} \tag{1}$$

$$E = \frac{(C_0 - C_e)}{C_0} \times 100 \tag{2}$$

where C_0 and C_e are the P concentrations (mg P/L) in the initial solution and filtrate, respectively; V is the volume of the solution (L); and m is the dry mass of adsorbent (g).

Adsorption isotherms

Isothermal adsorption experiments were carried out in shakers at 298, 308 and 318 K with different initial concentrations of P ranging from 20 to 60 mg P/L. After 0.02 g LC was added to the flask containing 100 mL P solution, the mixture was shaken at the desired temperature for 24 h. Then, the equilibrium data were measured and fitted with both Langmuir and Freundlich isotherm models as given by Equations (3) and (4), respectively:

$$\frac{C_e}{q_e} = \frac{1}{q_m K_L} + \frac{C_e}{q_m} \tag{3}$$

$$\mathrm{In}\ q_e = n\mathrm{In}\, C_e + \mathrm{In}\, K_F \tag{4}$$

where C_e is the concentration of P solution at equilibrium (mg P/L); q_e is the corresponding adsorption capacity (mg P/g); q_m (mg/g) and K_F (mg/g) are the constants in the Langmuir and Freundlich isotherm models, respectively, related to the adsorption capacity; K_L (L/mg) is the constant in the Langmuir isotherm model related to energy or net enthalpy of adsorption; and n is the constant in the Freundlich isotherm model that measures the adsorption intensity.

Kinetic studies

Kinetic tests were carried out in a 500 mL conical flask into which 200 mL of P solution and 0.04 g or 0.10 g of LC were added. The initial P concentrations were 20 and 50 mg P/L. The covered flask was shaken in a thermostatic chamber at 298 K for 24 h at 250 rpm. After each specified reaction time, a 1 mL sample was removed for analysis. The sample was then filtered through a 0.45 μm syringe nylon-membrane filter and the filtrate was analyzed for P concentration.

The experimental data were fitted with pseudo-first-order and pseudo-second-order models, described by Equations (5) and (6), respectively:

$$q_t = q_e(1 - e^{-k_1 t}) \tag{5}$$

$$\frac{t}{q_t} = \frac{1}{q_e}t + \frac{1}{k_2 q_e^2} \tag{6}$$

where q_t and q_e are the amounts of P adsorbed over a given period of time t (mg P/g) and at equilibrium (mg P/g), respectively; t is the adsorption time (h); and k_1 (1/h) and k_2 (g/(mg·h) are the adsorption rate constants of the pseudo-first-order adsorption and the pseudo-second-order adsorption, respectively.

pH studies

The effect of solution pH on P removal was investigated in the same way as for the adsorption measurements. The initial P concentration was 20 mg P/L, with pH ranging from 3.0 to 11.0. The suspensions were adjusted to the desired pH values with 0.1 M HCl or NaOH. Then, 0.02 g LC was added to the flask containing 100 mL P solution. The covered flask was shaken in an incubator shaker at 298 K for 24 h. The equilibrium pH was measured, and the suspension was centrifuged and analyzed for the residual P concentration in the supernatant.

Effect of the water matrix

To study the effect of common anions on P removal efficiency, 0.02 g LC was added into 100 mL P solution containing 0.01 M coexisting ions that were prepared by dissolving sodium salt forms of F^-, Cl^-, NO_3^-, SO_4^{2-}, and HCO_3^- into 20 mg P/L solution. After the covered flasks were shaken for 24 h at 298 K, the suspensions were filtered, and the filtrate was analyzed for P concentration.

P removal from the effluent wastewater

To mimic the typical P concentration of real wastewater, an initial P concentration of 3.2 mg P/L effluent was selected to demonstrate the applicability of LC nano-adsorbents. All batch adsorption experiments were investigated in the same way as for the adsorption measurements. After adding various amounts of LC to the flask containing 100 mL P solution, the covered flask was shaken in an incubator shaker at 298 K for 24 h. The suspension was then centrifuged and analyzed for the residual P concentration.

RESULTS AND DISCUSSION

Optimal experimental parameters for the preparation of LC

Effect of Mg-to-La molar ratio

The morphology and structural characteristics of LC obtained under various Mg^{2+} concentrations are summarized in Figure 1. For comparison, the XRD patterns of LC_0, which was prepared without the coexistence of Mg^{2+}, is also illustrated in Figure 1. Compared with the hexagonal layered structure of LC_0 (Figure 1(a)), SEM results for LC showed a dependence on the molar ratio of $C(Mg^{2+})/C(La^{3+})$. When the molar ratio of $C(Mg^{2+})/C(La^{3+})$ increased from 0.05:1 to 10:1(Figure 1(b)–1(d)), the particle size of LC was reduced from hundreds of nanometers to tens of nanometers. Although all LC samples maintained a layered nanostructure similar to LC_0, the shapes of each sample became more irregular and smaller with increasing Mg to La molar ratio, indicating that coexistence of Mg was a significant parameter for controlling the LC nanostructure.

Effect of reaction temperature

The structure of LC prepared at different reaction temperatures was also confirmed by XRD analysis (Figure 2(a)). A sharp peak at 10.27°, which is the most characteristic reflection of $La_2(CO_3)_3{\cdot}8H_2O$ (PDF #25-1400) and corresponding to the (002) plane, was observed in all samples, indicating the successful synthesis of LC nano-adsorbents. Other broad peaks were located at 18.51°, 20.79°, 21.24°, 27.08°, and 29.06°, corresponding to the (020), (004), (022), (220) and (222) reflections of $La_2(CO_3)_3{\cdot}8H_2O$, respectively. Since there were no peaks corresponding to $MgCO_3$ or

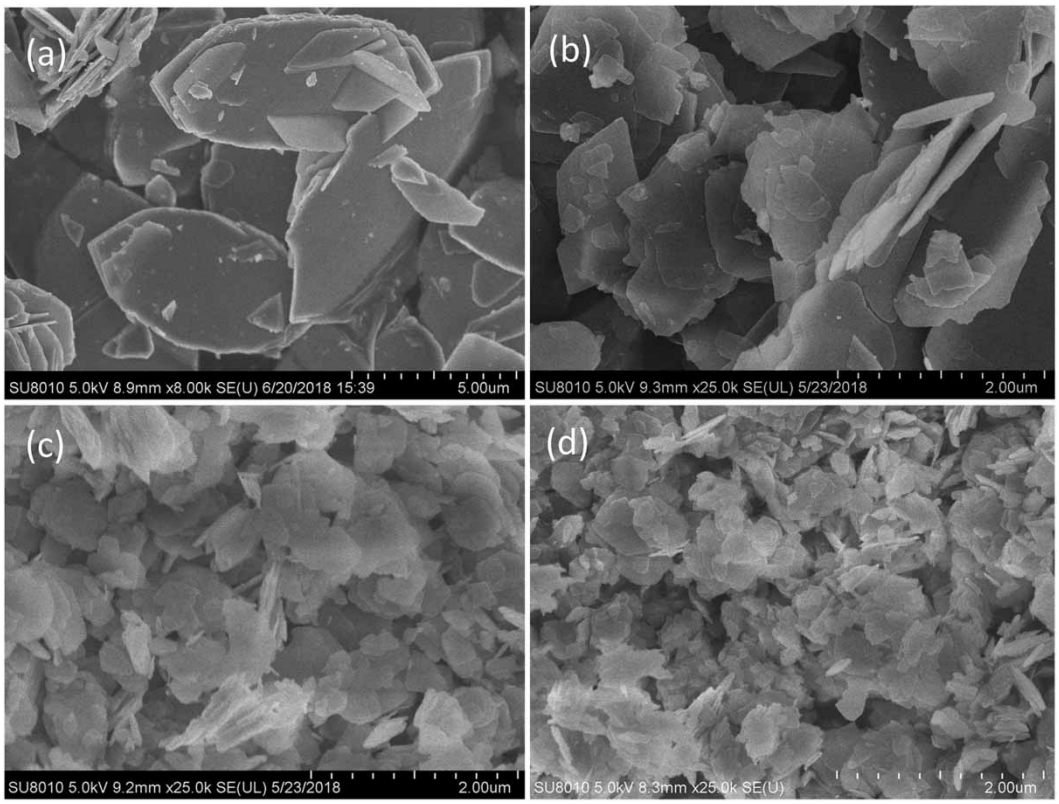

Figure 1 | SEM images of LC prepared with different Mg-to-La molar ratios of (a) 0:1, (b) 0.05:1, (c) 1:1 and (d) 10:1. Experimental conditions: $C(La^{3+}) = 0.04$ mol/L, $T = 298$ K.

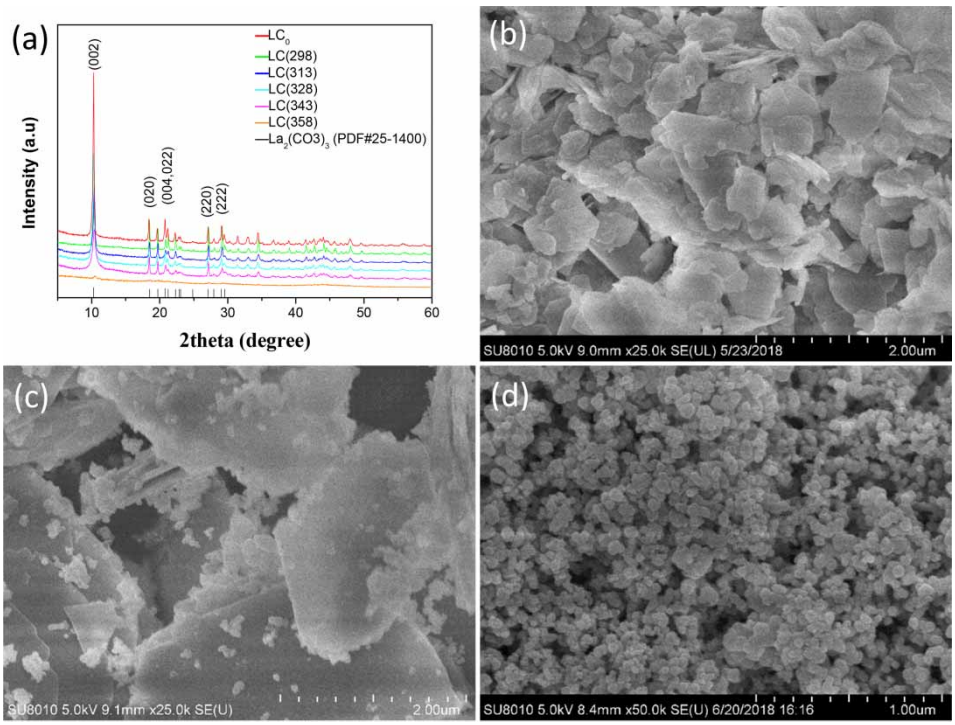

Figure 2 | (a) XRD patterns of LC_0 and LC prepared at 298 K, 313 K, 328 K, 343 to 358 K, denoted as LC(298), LC(313), LC(328), LC(343) and LC(358), respectively. (b-d) SEM images of LC prepared at 313, 343 and 358 K. Experimental conditions: $C(La^{3+}) = 0.04$ mol/L, $Mg^{2+}/La^{3+} = 1$ (mol/mol).

$La(OH)_3$ in Figure 1, it was reasonable to consider that the resulting product consisted only of LC. After the preparation temperature changed from 298 to 358 K, it was noted that there was a broadened and weakened peak at 10.27°, indicating that the prepared LC gradually lost its crystallinity with increased temperature. When the temperature reached 358 K, LC was completely transformed into an amorphous nanostructure. Since the amorphous phase is considered to be more favorable than the crystalline phase in P adsorption, the preparation of LC with this microscopic morphology should be more effective in removing P (Yang *et al.* 2017).

The SEM results of LC samples confirmed the same conclusions as from the preparation temperature (Figure 2(b)–2(d)). When the preparation temperature was between 298 and 313 K, LC had a well-defined layered structure, with the diameter ranging from 200 to 500 nm. Continuing to raise the preparation temperature to 328 K (Figure 2(c)), some small particles appeared and aggregated on the residual layered structure of LC. As the reaction temperature reached 358 K (Figure 2(d)), LC completely transformed into spherical nanometer microspheres with a uniform particle size of about 60 nm.

Zeta (ζ) potential analysis

Zeta (ζ) potential analysis was employed to determine the pH at the point of zero charge (pH_{pzc}). As shown in Figure 3, the pH_{pzc} of LC was 8.9. Compared with the value of LC_0 ($pH_{pzc} = 7.3$) and other La-incorporated materials reported in previous studies (He *et al.* 2016), the pH_{pzc} of LC shifted towards more alkaline conditions. In the case where the pH of the solution was lower than the pH_{pzc} of LC, the overall surface of LC would be protonated and positively charged, leading to static electric forces between positive LC and negative phosphate ions. While the pH value of the solution was higher than the pH_{pzc}, the functional groups of LC would gradually deprotonate and form a negative charge, causing electrostatic repulsion between the negatively charged surface sites and electronegative P species, thereby greatly reducing the adsorption of P on LC.

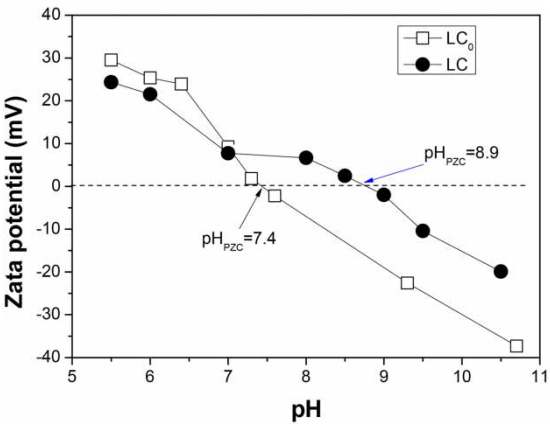

Figure 3 | The zeta potential of LC and LC_0 as a function of pH.

Batch adsorption experiments

Adsorption kinetics

Adsorption kinetics are used to evaluate the efficiency of adsorption between an adsorbent and adsorbate. The kinetic experiments with LC were conducted at two initial P concentrations of 20 mg P/L and 50 mg P/L. From Figure 4(a), it can be seen that P adsorption onto LC was divided into two stages: an initial rapid stage followed by a gradually slower stage until the adsorption equilibrium was achieved. In the rapid stage, P removal increased rapidly during the first 2 h, with a P adsorption capacity of 98.1 mg P/g in the 20 mg P/L solution and 111.8 mg P/g in the 50 mg P/L solution. Thereafter, the increase in contact time did not significantly increase the adsorption capacity of LC, and P was slowly adsorbed during the final reaction period. In contrast, the P adsorption onto LC_0 reached equilibrium after about 12 h and then increased slightly, resulting in a P adsorption capacity of 97.4 mg P/g in the 20 mg P/L solution and 105.4 mg P/g in the 50 mg P/L solution. The kinetic characteristics of LC; that is, the shortened equilibrium time and increased adsorption capacity, were attributed to the smaller nanoparticle size and higher pH_{pzc} value that helped LC have more active sites and much stronger forces that enhanced the interaction between LC and P.

To further study the P adsorption onto LC, the kinetic data recorded with different initial concentrations was fitted to the pseudo-first-order and pseudo-second-order models (Figure 4(b)–4(c)). The corresponding parameters and correlation coefficients are listed in Table 1. According to the correlation coefficients, the pseudo second-order model simulated the P adsorption process better than the pseudo first-order model, suggesting that chemisorption or chemical bonding between adsorbent active sites and P might dominate the adsorption process. Based on the rate constants of the pseudo second-order model (0.392 and 0.299 g/(mg·h) for initial P concentrations of 20 and 50 mg P/L, respectively), less time was needed for LC to achieve

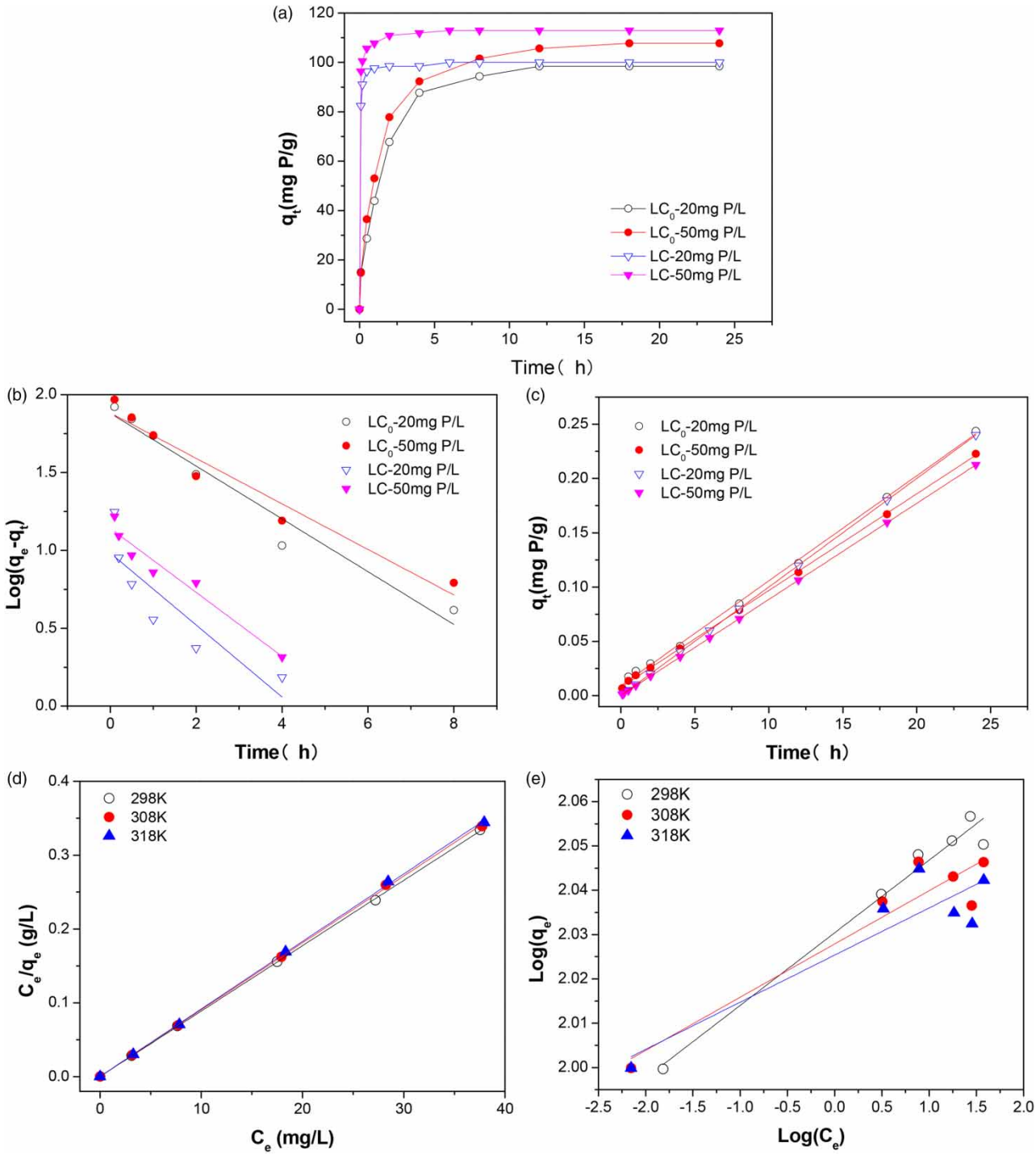

Figure 4 | Phosphate adsorption. (a) adsorption performance of P onto LC as a function of contact time; (b) and (c) results of two kinetic models of pseudo-first-order and pseudo-second-order, respectively; (d) and (e) results of Langmuir and Freundlich isotherm models, respectively. Experimental conditions for (a), (b) and (c) 20 and 50 mg P/L, 0.2 g/L of adsorbent dosage, pH 6.5 ± 0.1, T = 298 K, contact time 24 h ; (d) and (e) 20 mg P/L, 0.2 g/L of adsorbent dosage, pH 6.5 ± 0.1, T = 298, 308 and 318 K, contact time 24 h.

effective P removal. This performance result is beneficial for potential applications, as the rapid adsorption process can shorten the dephosphorization time in water and wastewater treatment.

Adsorption isotherms

Based on the optimized conditions, the adsorption isotherms were studied at 298, 308 and 318 K and the results

Table 1 | The pseudo-first-order and pseudo-second-order model constants and correlation coefficients using LC and LC_0 for P removal at different initial P concentrations

		Pseudo-first-order			Pseudo-second-order		
Adsorbents	**Initial concentration C_0 (mg P/L)**	**k_1 (1/h)**	**q_e (mg/g)**	**R^2**	**k_2 (g/mg·h)**	**q_e (mg/g)**	**R^2**
LC_0	20	0.390	75.9	0.9559	0.010	103.4	0.9986
	50	0.337	76.4	0.9465	0.010	112.5	0.9997
LC	20	0.532	9.6	0.7278	0.392	100.1	0.9999
	50	0.473	13.9	0.9389	0.299	113.1	0.9999

are shown in Figure 4(d) and 4(e). The adsorption data were further fitted by Langmuir and Freundlich models, and the obtained parameters are reported in Table 2. The P adsorption isotherms were better fitted by the Langmuir model ($R^2 > 0.9997$) than the Freundlich model ($R^2 > 0.7961$), suggesting a monolayer P adsorption onto LC. The maximum adsorption capacities (q_m) estimated by the Langmuir model were 112.9 mg P/g, 110.5 mg P/g, and 109.4 mg P/g at 298 K, 308 K, and 318 K, respectively. It is thus reasonable to consider that the adsorption process on LC should be exothermic in nature.

Compared with the q_m values of other reported La-modified adsorbents (Table 3), the fact that the P adsorption capacity of LC was higher than those reported for lanthanum hydroxide (107.5 mg P/g) (Xie *et al.* 2014b) and lanthanum oxide (47.0 mg P/g) (Xie *et al.* 2015), demonstrated the superiority of LC for P removal.

Adsorption thermodynamics

The thermodynamic parameters in the progress of P adsorption on the adsorbent of LC at different temperatures (298, 308, and 318 K), including the change of Gibbs free energy (ΔG°, kJ/mol), enthalpy (ΔH°, kJ/mol), and entropy (ΔS°, J/mol·K), were calculated by the following equations:

$$K_d = \frac{q_e}{C_e} \tag{7}$$

$$InK_d = \frac{\Delta S^0}{R} - \frac{\Delta H^0}{RT} \tag{8}$$

Table 2 | Langmuir and Freundlich isotherm parameters of P adsorption for LC at 298 K, 308 K, and 318 K

		Langmuir				Freundlich		
Adsorbents	**T (K)**	**q_m (mg/g)**	**K_L (L/mg)**	**R_L**	**R^2**	**n**	**K_F (mg/g)**	**R^2**
LC (pH = 6.5)	298	112.9	29.96	0.00056	0.9999	0.0164	107.3	0.9697
	308	110.5	28.89	0.00058	0.9997	0.0120	106.6	0.8759
	318	109.4	27.34	0.00061	0.9997	0.0106	106.0	0.7961

Table 3 | Comparison of P adsorption capacity of different La-based adsorbents*

Adsorbents		**La/%**	**Adsorption capacity (mg P/g)**	**References**
$La(OH)_3$-modified EV	3.0–7.0	41..5	79.6	Huang *et al.* (2014a)
C-$La(OH)_3$	2.5–9.0	71.0	55.6	Xie *et al.* (2014b)
C-La_2O_3	<~ 10.5	85.3	47.0	Xie *et al.* (2015)
M-$La(OH)_3$	2.5–12.0	58.0	107.5	Xie *et al.* (2014b)
MCH-$La(OH)_3$-EW	4.5–11	42.9	90.2	Dong *et al.* (2017)
La-doped SiO_2	3.0–8.0	22.4	47.9	Huang *et al.* (2014b)
La metal-organic frameworks	NA	NA	173.8	Zhang *et al.* (2017)
Magnetite/$La(OH)_3$	7.0	34.9	52.7	Fang *et al.* (2018)
LC	3.0–11.0	46.0	112.9	This work

NA = Not available.
*Values from the literature are provided for comparison.

$$\Delta G = -RTInK_d \tag{9}$$

where K_d is the thermodynamic equilibrium constant of the adsorption process; q_e (mg P/g) is the amount adsorbed on solid at equilibrium; C_e (mg P/L) is the equilibrium concentration; R (8.314 J/mol·K) is the universal gas constant; and T (K) is the absolute temperature.

All the thermodynamic parameters are listed in Table 4. The negative ΔG values indicated that the adsorption process of phosphate was spontaneous under the experimental conditions. The value of ΔH° was negative in the temperature range of 298–318 K, confirming that the adsorption process of P on LC is exothermic in nature. The result was supported by the decrease in the adsorption capacity of P with the ascending temperature (Table 2). The positive value of ΔS° indicates that the adsorption process increased the degrees of freedom of the system.

Physical models

A monolayer model for single adsorption was selected and analyzed to explain the experimental adsorption data. It was assumed that P removal was caused by a monolayer process with one adsorption energy that described the interactions between P and the LC adsorbent. The expression of this monolayer adsorption model is given by the following equation:

$$Q_e = \frac{nD_m}{1 + \left(\frac{C_{1/2}}{C_e}\right)^n} \tag{10}$$

where parameter n is the number of linked P per the functional group of LC adsorbent, and D_m is the functional group density that can be obtained at saturation. The product of these parameters is the adsorption capacity at saturation that can be calculated via the relationship $Q_s = n{\cdot}D_m$. $C_{1/2}$ is the concentration at half-saturation.

The parameter n is a stoichiometric coefficient that can provide additional information to interpret the adsorption mechanisms of P on LC. Referring to the values listed in Table 5, it was found in single adsorption systems that the temperature had a positive effect on this parameter, which increased with the adsorption temperature from 308 to 318 K. Moreover, all estimated values of n were less than 0.5, indicating that P can be shared on at least two functional groups of LC. In contrast, the increment of temperature caused a decrement of the parameter D_m. This trend has two possible explanations: (1) an increment of the parameter n led to a decrement of the density of functional groups, or (2) the thermal collisions affected and reduced the occupied adsorption functional groups.

Table 4 | Thermodynamic data for P adsorption onto LC

Temperature (K)	ΔH° (kJ/mol)	ΔS° (J/mol·K)	ΔG° (kJ/mol)
298	−2.34	21.75	−8.82
308			−9.04
318			−9.26

Application evaluation

Effect of solution pH

pH is an essential parameter in optimizing chemical processes for removing ions from aqueous solutions. Due to the competition between hydroxyl ions and the phosphate ions on the surface of the adsorbent, P uptake usually increases with the decrease of pH. However, as shown in Figure 5, LC performed well for P removal over a wide pH

Table 5 | Parameters of statistical physics models for the adsorption of P on LC

T (K)	n	D_m (mg/g)	$C_{1/2}$ (mg/L)	Q_s (mg/g)
298	0.128	965.39	2.64×10^{-7}	123.6
308	0.298	375.70	8.18×10^{-6}	112.0
318	0.471	232.55	6.69×10^{-5}	109.5

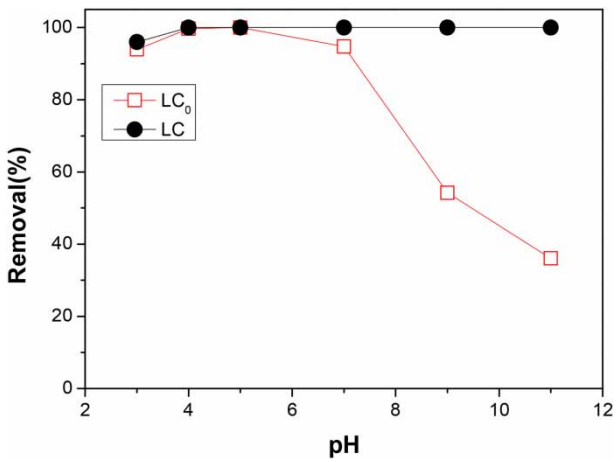

Figure 5 | Adsorption of P onto LC and LC_0 as a function of initial P solution pH (T = 298 K, reaction time = 24 h, adsorbent dosage of 0.2 g/L for initial P concentration of 20 mg P/L solution).

range. For example, when the solution pH was increased from 4.0 to 11.0, the removal efficiency reached almost 99% at the initial P concentration of 20 mg P/L. The fact that LC showed high removal efficiency under both acidic and alkaline conditions indicates that LC could overcome the limitations of use under acidic conditions and show strong and stable P removal capacity over a wide pH range.

For comparison purposes, the results of pH on LC_0 are also given in Figure 5. Since it is generally believed that the adsorption reactions at lower pH are much more favorable than the adsorption reactions at higher pH values (Fang *et al.* 2017), it is not surprising that acidity was the most favorable condition for P removal by LC. The adsorption efficiency approached 93% at pH of 3.0–7.0. The P removal efficiency then decreased sharply to 36% with increasing pH from 7.0 to 11.0. Compared with other lanthanum-containing materials, similar results have been observed concerning the effect of pH for P removal (Liu *et al.* 2011; Qiu *et al.* 2015; Zhang *et al.* 2016).

As the pH_{pzc} value increased, the surface charge of LC tended to change from negative to positive. As such, more $H_2PO_4^-$ and HPO_4^{2-} could be captured onto LC through electrostatic attraction and ligand exchange (Tokunaga *et al.* 1997; Chen *et al.* 2012). Benefiting from both the proper P species distribution and the large Zeta (ζ) potential of LC versus pH, LC could exhibit high P adsorption capacity of negatively charged phosphate over a wide pH tolerance range.

Effect of adsorbent dosage

The influence of adsorbent dosage on P removal was investigated as the amount of LC varied from 0.025 to 0.30 g/L. Increased adsorbent dosage implied a greater surface area and a greater number of P binding sites available. As shown in Figure 6, P removal increased sharply with increasing LC dose from 0.025 to 0.20 g/L. Thereafter, the removal efficiency of P increased slowly and approached the maximum value of 99.9% for an initial P concentration of 10 mg P/L.

The effect of dosage on adsorption capacity is also presented in Figure 6. When the dosage varied from 0.025 to 0.15 g/L, the adsorption capacity of LC remained almost unchanged. As the dosage increased and became greater than 0.15 g/L, the adsorption capacity was reduced by 86%. Since there was an intersection between the P removal curve and the adsorption capacity curve, the optimal value of LC could be obtained so as to have both high P adsorption capacity and removal efficiency. As a result, the dosage selected was 0.15–0.20 g/L for further studies.

Effect of coexisting ions

Coexisting anions, such as F^-, Cl^-, SO_4^{2-}, NO_3^-, and HCO_3^-, are commonly present with P in natural water and wastewater. These anions could potentially compete with phosphate for the adsorption sites. The interferences of coexisting anions, including F^-, Cl^-, SO_4^{2-}, NO_3^-, and HCO_3^-, were studied in the experiment. To simulate the real wastewater conditions, the concentration of co-existing ions was 0.01 M, which was 10 times the initial concentration of P. From the results shown in Figure 7, it can be seen that F^-, Cl^-, SO_4^{2-} and NO_3^- had no, or only just a slight influence on the P adsorption, suggesting that such anions, even at relatively high concentrations, did not

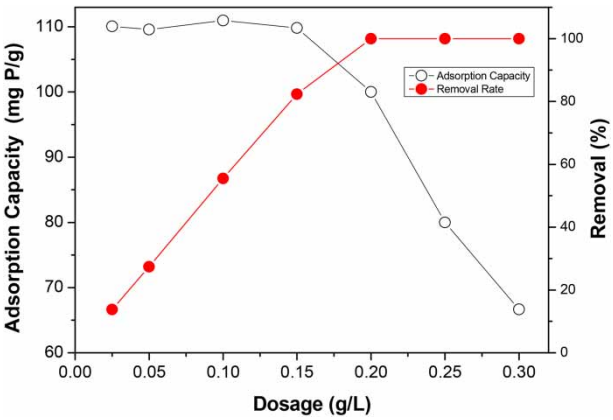

Figure 6 | The effect of dosage of LC on the P adsorption performance (pH = 6.5, T = 298 K, reaction time = 24 h).

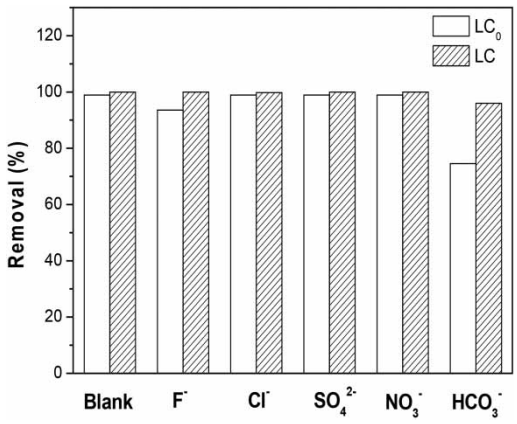

Figure 7 | Effect of coexisting anions on the P removal efficiencies by using LC and LC_0 (T = 298 K, pH = 6.5, adsorbent dosage = 0.2 g/L, reaction time = 24 h, C_0 = 1 mg P/L).

present significant competition to the P adsorption on LC. However, the P removal efficiency of LC_0 was reduced by 25% in 0.01 M HCO_3^- solution. This conclusion agreed well with a previous study on P removal by La-based materials (Koilraj & Sasaki 2017), indicating that LC also possesses strong selectivity towards P, thereby offering great support in the practical utilization for effluent wastewater treatment.

Real sewage treatment performance

To evaluate the practicability of the prepared LC for real sewage treatment, LC was applied to domestic wastewater containing low concentration P. The initial concentration of P in the collected sewage sample was about 3.2 mg P/L. The evolution of P concentration after being treated by different doses of LC is shown in Figure 8. A small dose of 0.5 g/L LC realized the removal of P pollutants to less than 0.5 mg P/L, fully meeting the discharge standard of China (0.5 mg total P/L) (Wu *et al.* 2017). The relatively low dose and satisfactory sewage treatment efficiency indicated that LC is a promising candidate for the practical water purification process.

Phosphate removal mechanism

Multiple analytical methods (XRD, FTIR and SEAD) were utilized to investigate the mechanism of LC for superior adsorption performance.

The P adsorption mechanism was investigated by the microscopic technique of FTIR spectroscopy. Figure 9(a) shows the FTIR spectra of LC before and after P adsorption.

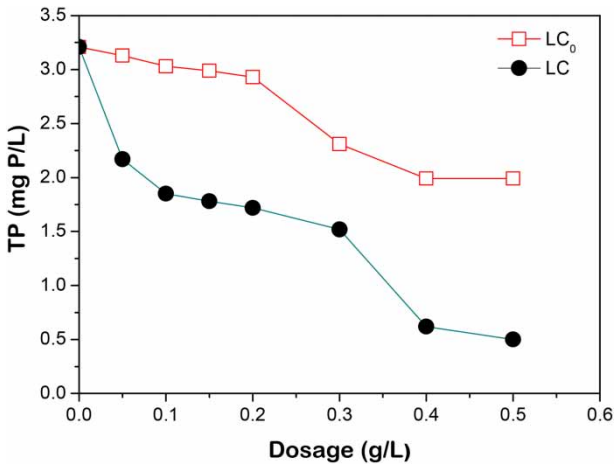

Figure 8 | P removal of real domestic wastewater by LC and LC_0.

Without P adsorption, the FTIR spectrum of LC had strong hydroxyl stretching (3,425 cm^{-1}) and bending (1,631 cm^{-1}) vibrations of physically adsorbed H_2O, and the strong antisymmetric stretching vibration (1,474 cm^{-1} and 1,369 cm^{-1}) and weak bending vibration (845 cm^{-1}) of CO_3^{2-}. After P adsorption, the intensities of all CO_3^{2-} peaks saw an obvious decline. At the same time, new sharp bands located at about 1,050 $cm^{-}1$, corresponding to the asymmetric vibration of P–O and $P=O$ bonds of PO_4^{3-}, appeared after adsorption, indicating that P was successfully captured by the adsorbent.

The XRD patterns of LC before and after P adsorption were further studied, and the results are depicted in Figure 9(b). There are typical changes of XRD diffraction peaks before and after P adsorption. The intensities of peaks representing LC were reduced, indicating their participation in the adsorption process. However, characteristic diffraction peaks assigned to $LaPO_4{\cdot}xH_2O$ at $2\theta = 14.6°$, 29.5° and 41.5° were also observed (Zhang *et al.* 2016). The appearance of La phosphate compounds after adsorption indicated that P anions in solution were combined with La cations on LC that contributed to the phosphate removal from the solutions.

The corresponding selected area electron diffraction pattern (SAED) is also shown in Figure 9(c) and 9(d). Before dephosphorization, a series of concentric rings in the SAED pattern indicated that the prepared LC may have an amorphous structure. After dephosphorization, the corresponding spot ring SAED pattern can be indexed as a mixed structure of single crystal and polycrystalline nanoparticles.

CONCLUSIONS

Many researchers have investigated the effect of pH on P adsorption capacity and found that lanthanum-based adsorbents have high P removal efficiencies only at lower pH values. In order to obtain a highly efficient adsorbent for P removal under neutral and alkaline conditions, LC nanoadsorbents were prepared in the presence of Mg^{2+} cations at different temperatures. Characterization results revealed that an amorphous structure and nanoparticle size were highly effective for LC dephosphorization. The optimal conditions for the synthesis of LC were a ratio of 1:1 (mol/mol) for Mg^{2+} to La^{3+}, 0.04 M $LaCl_3$ concentration, and at a 358 K reaction temperature. Batch adsorption results showed that the maximum P adsorption capacity of LC was 112.9 mg P/g. In a 20 mg P/L solution, the P adsorption

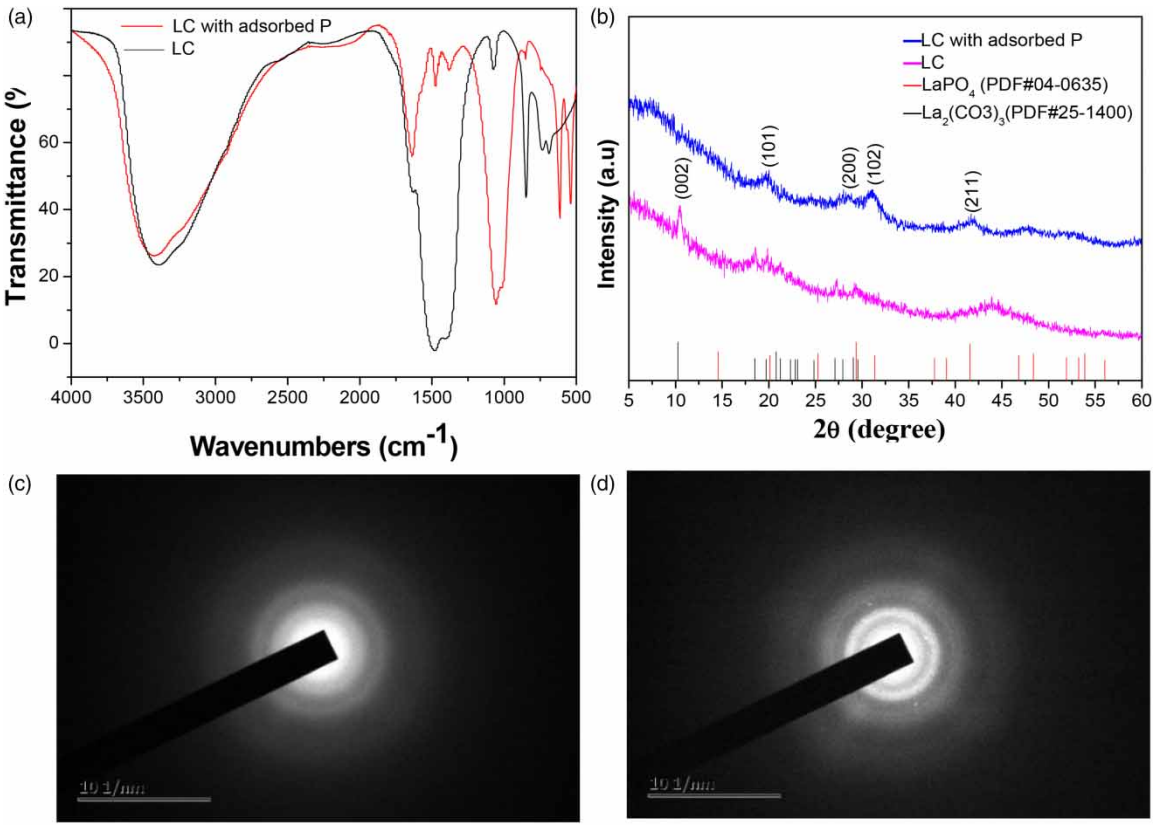

Figure 9 | (a) FTIR spectra, (b) XRD patterns (c) SAED pattern of LC, and (d) SAED pattern of LC with adsorbed P.

equilibrium was reached within 2 h with an adsorbent dosage of 0.2 g/L. LC exhibited high P removal performance over a wide pH range from 3.0 to 11.0 as well as excellent selectivity for P in the presence of common competing ions. Thermodynamic analyses indicated that the phosphate adsorption process was exothermic and spontaneous in nature. Results of statistical physics modeling suggested that P can fully interact with two or more functional groups from the adsorbent surface. The analysis also demonstrated the feasibility for real sewage treatment, residual P concentration in sewage could be decreased to below 0.5 mg P/L, meeting the stringent criterion for eutrophication prevention. In summary, LC can serve as a promising adsorbent for efficient and preferable P removal under a wide range of pH conditions.

ACKNOWLEDGEMENTS

This work was financially supported by the Major Science and Technology Program for Water Pollution Control and Treatment, China (2018ZX07208). We thank LetPub (www.letpub.com) for its linguistic assistance and scientific consultation during the preparation of this manuscript.

DATA AVAILABILITY STATEMENT

All relevant data are included in the paper or its Supplementary Information.

REFERENCES

Aneesh, P. K., Prathish, K. P., Kala, R. & Rao, T. P. 2009 Lanthanum carbonate incorporated chitosan microparticles for phosphate collection. *Reactive & Functional Polymers* **69**, 714–718.

Behets, G. J., Dams, G., Vercauteren, S. R., Damment, S. J., Bouillon, R., De Broe, M. E. & D'Haese, P. C. 2004 Does the phosphate binder lanthanum carbonate affect bone in rats with chronic renal failure? *Journal of the American Society of Nephrology* **15** (8), 2219–2228.

Bhardwaj, D., Sharma, P., Sharma, M. & Tomar, R. 2014 Removal and slow release studies of phosphate on surfactant loaded hydrothermally synthesized silicate nanoparticles. *Journal of*

the Taiwan Institute of Chemical Engineers **45** (5), 2649–2658.

Chen, N., Feng, C., Zhang, Z., Liu, R., Gao, Y., Li, M. & Sugiura, N. 2012 Preparation and characterization of lanthanum(III) loaded granular ceramic for phosphorus adsorption from aqueous solution. *Journal of the Taiwan Institute of Chemical Engineers* **43**, 783–789.

Chouyyok, W., Wiacek, R. J., Pattamakomsan, K., Sangvanich, T., Grudzien, R. M., Fryxell, G. E. & Yantasee, W. 2010 Phosphate removal by anion binding on functionalized nanoporous sorbents. *Environmental Science & Technology* **44** (8), 3073–3078.

Correll, D. L. 1998 The role of phosphorus in the eutrophication of receiving waters: a review. *Journal of Environmental Quality* **27** (2), 261–266.

Ding, S. M., Chen, M. S., Gong, M. D., Fan, X. F., Qin, B. Q., Xu, H., Gao, S. S., Jin, Z. F., Tsang, D. C. W. & Zhang, C. S. 2018 Internal phosphorus loading from sediments causes seasonal nitrogen limitation for harmful algal blooms. *Science of the Total Environment* **625**, 872–884.

Dodds, W. K., Bouska, W. W., Eitzmann, J. L., Pilger, T. J., Pitts, K. L., Riley, A. J., Schloesser, J. T. & Thornbrugh, D. J. 2009 Eutrophication of U.S. freshwaters: analysis of potential economic damages. *Environmental Science & Technology* **43** (1), 12–19.

Dong, S. X., Wang, Y. L., Zhao, Y. W., Zhou, X. H. & Zheng, H. L. 2017 $La^{3+}/La(OH)_3$ loaded magnetic cationic hydrogel composites for phosphate removal: effect of lanthanum species and mechanistic study. *Water Research* **126**, 433–441.

Dulekgurgen, E., Ovez, S., Artan, N. & Orhon, D. 2003 Enhanced biological phosphate removal by granular sludge in a sequencing batch reactor. *Biotechnology Letters* **25**, 687–693.

Fang, L., Shi, Q., Nguyen, J., Wu, B., Wang, Z. & Lo, I. M. C. 2017 Removal mechanisms of phosphate by lanthanum hydroxide nanorods: investigations using EXAFS, ATR-FTIR, DFT, and surface complexation modeling approaches. *Environmental Science & Technology* **51**, 12377–12384.

Fang, L. P., Liu, R., Li, J., Xu, C. H., Huang, L. Z. & Wang, D. S. 2018 Magnetite/Lanthanum hydroxide for phosphate sequestration and recovery from lake and the attenuation effects of sediment particles. *Water Research* **130**, 243–254.

Guo, H., Zhang, X. J., Tang, S. W. & Zhang, S. L. 2013 Effects and safety of lanthanum carbonate in end stage renal disease patients with hyperphosphatemia: a meta-analysis – system review of lanthanum carbonate. *Renal Failure* **35** (10), 1455–1464.

He, Y. H., Lin, H., Dong, Y. B., Liu, Q. L. & Wang, L. 2016 Simultaneous removal of ammonium and phosphate by alkaline-activated and lanthanum-impregnated zeolite. *Chemosphere* **164**, 387–395.

Huang, W. Y., Li, D., Liu, Z. Q., Tao, Q., Zhu, Y., Yang, J. & Zhang, Y. M. 2014a Kinetics, isotherm, thermodynamic, and adsorption mechanism studies of $La(OH)_3$-modified exfoliated vermiculites as highly efficient phosphate adsorbents. *Chemical Engineering Journal* **236** (2), 191–201.

Huang, W. Y., Zhu, Y., Tang, J. P., Yu, X., Wang, X. L., Li, D. & Zhang, Y. M. 2014b Lanthanum-doped ordered mesoporous hollow silica spheres as novel adsorbents for efficient phosphate removal. *Journal of Materials Chemistry A* **2** (23), 8839–8848.

Hussain, S., Aziz, H. A., Isa, M. H., Ahmad, A., Van Leeuwen, J., Zou, L., Beecham, S. & Umar, M. 2011 Orthophosphate removal from domestic wastewater using limestone and granular activated carbon. *Desalination* **271** (1–3), 265–272.

Hutchison, A. J., Wilson, R. J., Garafola, S. & Copley, J. B. 2016 Lanthanum carbonate: safety data after 10 years. *Nephrology* **21** (12), 987–994.

Karydis, M. & Kitsiou, D. 2012 Eutrophication and environmental policy in the Mediterranean Sea: a review. *Environmental Monitoring and Assessment* **184** (8), 4931–4984.

King, K. W., Williams, M. R., Macrae, M. L., Fausey, N. R., Frankenberger, J., Smith, D. R., Kleinman, P. J. A. & Brown, L. C. 2015 Phosphorus transport in agricultural subsurface drainage: a review. *Journal of Environmental Quality* **44** (2), 467–485.

Koilraj, P. & Sasaki, K. 2017 Selective removal of phosphate using La-porous carbon composites from aqueous solutions: batch and column studies. *Chemical Engineering Journal* **317**, 1059–1068.

Lee, Y. K., Choi, H. Y., Shin, S. K. & Lee, H. Y. 2013 Effect of lanthanum carbonate on phosphate control in continuous ambulatory peritoneal dialysis patients in Korea: a randomized prospective study. *Clinical Nephrology* **79** (2), 136–142.

Li, H., Ru, J. Y., Yin, W., Liu, X. H., Wang, J. Q. & Zhang, W. D. 2009 Removal of phosphate from polluted water by lanthanum doped vesuvianite. *Journal of Hazardous Materials* **168** (1), 326–330.

Liu, J. Y., Wan, L. H., Zhang, L. & Zhou, Q. 2011 Effect of pH, ionic strength, and temperature on the phosphate adsorption onto lanthanum-doped activated carbon fiber. *Journal of Colloid and Interface Science* **364** (2), 490–496.

Liu, J. Y., Zhou, Q., Chen, J. H., Zhang, L. & Chang, N. 2013 Phosphate adsorption on hydroxyl-iron-lanthanum doped activated carbon fiber. *Chemical Engineering Journal* **215**, 859–867.

Loganathan, P., Vigneswaran, S., Kandasamy, J. & Bolan, N. S. 2014 Removal and recovery of phosphate from water using sorption. *Critical Reviews in Environmental Science and Technology* **44** (8), 847–907.

Oka, Y., Matsuda, H. & Miyazaki, M. 2016 Did lanthanum carbonate improve prognosis in patients requiring chronic hemodialysis in the Kawashima study? *Therapeutic Apheresis and Dialysis* **20** (5), 538–539.

Qiu, H., Liang, C., Zhang, X. L., Chen, M. D., Zhao, Y. X., Tao, T., Xu, Z. W. & Liu, G. 2015 Fabrication of a biomass-based hydrous zirconium oxide nanocomposite for preferable phosphate removal and recovery. *ACS Applied Materials & Interfaces* **7** (37), 20835–20844.

Seminskaya, O. O., Balakina, M. N. & Kucheruk, D. D. 2017 Processing of retentates of reverse osmosis treatment of phosphate-containing wastewater. *Journal of Water Chemistry and Technology* **39** (3), 308–317.

Shao, H., Liu, Z., Li, M., Wu, J. & Hu, Y. 2011 Application of lanthanum carbonate in hyperphosphataemia treatment. *Chinese Rare Earths* **32** (1), 75–79.

Shepherd, J. G., Sohi, S. P. & Heal, K. V. 2016 Optimising the recovery and re-use of phosphorus from wastewater effluent for sustainable fertiliser development. *Water Research* **94**, 155–165.

Sidat, M., Kasan, H. C. & Bux, F. 1999 Laboratory-scale investigation of biological phosphate removal from municipal wastewater. *Water SA* **25** (4), 459–462.

Spears, B. M., Lürling, M., Yasseri, S., Castro-Castellon, A. T., Gibbs, M., Meis, S., McDonald, C., McIntosh, J., Sleep, D. & Van Oosterhout, F. 2013 Lake responses following lanthanum-modified bentonite clay (Phoslock®) application: an analysis of water column lanthanum data from 16 case study lakes. *Water Research* **47** (15), 5930–5942.

Tian, S. L., Jiang, P. X., Ning, P. & Su, Y. H. 2009 Enhanced adsorption removal of phosphate from water by mixed lanthanum/aluminum pillared montmorillonite. *Chemical Engineering Journal* **151** (1–3), 141–148.

Tokunaga, S., Wasay, S. A. & Park, S. W. 1997 Removal of arsenic(V) ion from aqueous solutions by lanthanum compounds. *Water Science and Technology* **35**, 71–78.

Tonelli, M., Pannu, N. & Manns, B. 2010 Drug therapy: oral phosphate binders in patients with kidney failure. *New England Journal of Medicine* **362** (14), 1312–1324.

Wang, X., Wang, Y., Zhang, X., Feng, H., Li, C. & Xu, T. 2013 Phosphate recovery from excess sludge by conventional electrodialysis (CED) and electrodialysis with bipolar membranes (EDBM). *Industrial & Engineering Chemistry Research* **52** (45), 15896–15904.

Wang, Z., Fan, Y., Li, Y. W., Qu, F. R., Wu, D. Y. & Kong, H. N. 2016 Synthesis of zeolite/hydrous lanthanum oxide composite from coal fly ash for efficient phosphate removal from lake water. *Microporous and Mesoporous Materials* **222**, 226–234.

Wu, P., Wu, J. S., Xia, L., Liu, Y., Xu, L. Y. & Song, S. X. 2017 Adsorption of fluoride at the interface of water with calcined magnesium-ferri-lanthanum hydrotalcite-like compound. *RSC Advances* **7** (42), 26104–26112.

Xie, J., Wang, Z., Fang, D., Li, C. J. & Wu, D. Y. 2014a Green synthesis of a novel hybrid sorbent of zeolite/lanthanum hydroxide and its application in the removal and recovery of phosphate from water. *Journal of Colloid and Interface Science* **423**, 13–19.

Xie, J., Wang, Z., Lu, S. Y., Wu, D. Y., Zhang, Z. J. & Kong, H. N. 2014b Removal and recovery of phosphate from water by lanthanum hydroxide materials. *Chemical Engineering Journal* **254**, 163–170.

Xie, J., Lin, Y., Li, C. J., Wu, D. Y. & Kong, H. N. 2015 Removal and recovery of phosphate from water by activated aluminum oxide and lanthanum oxide. *Powder Technology* **269** (4), 351–357.

Yan, L. G., Xu, Y. Y., Yu, H. Q., Xin, X. D., Wei, Q. & Du, B. 2010 Adsorption of phosphate from aqueous solution by hydroxy-aluminum, hydroxy-iron and hydroxy-iron-aluminum pillared bentonites. *Journal of Hazardous Materials* **179** (1–3), 244–250.

Yang, J., Zhou, L., Zhao, L. Z., Zhang, H. W., Yin, J. N., Wei, G. F., Qian, K., Wang, Y. H. & Yu, C. Z. 2011 A designed nanoporous material for phosphate removal with high efficiency. *Journal of Materials Chemistry* **21** (8), 2489–2494.

Yang, Q., Wang, X. L., Luo, W., Sun, J., Xu, Q. X., Chen, F., Zhao, J. W., Wang, S. N., Yao, F. B. & Wang, D. B. 2017 Effectiveness and mechanisms of phosphate adsorption on iron-modified biochars derived from waste activated sludge. *Bioresource Technology* **247**, 537–544.

Yue, Q. Y., Zhao, Y. Q., Li, Q., Li, W. H., Gao, B. Y., Han, S. X., Qi, Y. F. & Yu, H. 2010 Research on the characteristics of red mud granular adsorbents (RMGA) for phosphate removal. *Journal of Hazardous Materials* **176** (1–3), 741–748.

Zhang, J. D., Shen, Z. M., Shan, W. P., Mei, Z. J. & Wang, W. H. 2011 Adsorption behavior of phosphate on lanthanum(III)-coordinated diamino-functionalized 3D hybrid mesoporous silicates material. *Journal of Hazardous Materials* **186** (1), 76–83.

Zhang, Y. Y., Pan, B. C., Shan, C. & Gao, X. 2016 Enhanced phosphate removal by nanosized hydrated La(III) oxide confined in cross-linked polystyrene networks. *Environmental Science & Technology* **50** (3), 1447–1454.

Zhang, X. T., Sun, F. L., He, J. J., Xu, H. B., Cui, F. Y. & Wang, W. 2017 Robust phosphate capture over inorganic adsorbents derived from lanthanum metal organic frameworks. *Chemical Engineering Journal* **326**, 1086–1094.

First received 27 November 2020; accepted in revised form 14 February 2021. Available online 1 March 2021